An Alternative Analysis of the LSND Neutrino Oscillation Search Data on $\overline{\nu}_\mu \longrightarrow \overline{\nu}_e$

James E. Hill

University of Pennsylvania, Philadelphia, Pennsylvania 19104

(Received 18 April 1995; revised manuscript received 28 June 1995)

This analysis of data from the Liquid Scintillator Neutrino Detector (LSND) at the Los Alamos Meson Physics Facility (LAMPF) sets bounds on neutrino oscillations in the appearance channel $\overline{\nu}_\mu \rightarrow \overline{\nu}_e$ by searching for the signature of the reaction $\overline{\nu}_e p \rightarrow e^+ n$: an e^+ followed by a 2.2 MeV γ ray from neutron capture. Five $e^{\pm}$-γ coincidences are observed in time with the LAMPF beam, with an estimated background of 6.2 events. The 90% confidence limits obtained in this analysis are $\Delta m^2 < 0.07$ eV^2 for $\sin^2 2\theta = 1$, and $\sin^2 2\theta < 6 \times 10^{-3}$ for $\Delta m^2 \gtrsim 20$ eV^2. The possible signal at the edge of the detector's sensitivity is mentioned.

PACS numbers: 14.60.Pq, 13.15.+g

The phenomenon of neutrino oscillations [1,2] is a sensitive probe of finite masses in the neutral lepton sector, the only remaining elementary fermions with unknown masses. With a few simplifying assumptions, the probability P of oscillations $\overline{\nu}_\mu \rightarrow \overline{\nu}_e$ can be written $P_{\overline{\nu}_\mu \rightarrow \overline{\nu}_e} = \sin^2(2\theta)\sin^2\{1.27\Delta[m^2(\mathrm{eV}^2)]L(\mathrm{m})/E(\mathrm{MeV})\}$. Accelerator experiments may probe very low $[\mathcal{O}(10^{-3})]$ values of mixing strength, $\sin^2 2\theta$, and mass splittings $\Delta m^2 \approx |m^2_{\overline{\nu}_\mu} - m^2_{\overline{\nu}_e}| \gtrsim \mathcal{O}(10^{-2}\ \mathrm{eV}^2)$ by searches for appearance of $\overline{\nu}_e$ in a high intensity $\overline{\nu}_\mu$ beam.

The Liquid Scintillator Neutrino Detector (LSND) was built at the Los Alamos Meson Physics Facility (LAMPF) in part to search for oscillations $\overline{\nu}_\mu \rightarrow \overline{\nu}_e$. The $\overline{\nu}_e$ is detected via the weak charged current interaction $\overline{\nu}_e p \rightarrow e^+ n$. For $\overline{\nu}_e$ resulting from the $\overline{\nu}_\mu$ from muon decay at rest, this interaction will produce a continuous positron spectrum up to 50 MeV, which can be loosely tagged by a delayed time coincidence with the 2.2 MeV γ ray emitted after neutron capture on hydrogen in the detector mineral oil. Since the detector is insensitive to the charge of a particle, the search is performed above the 35 MeV end point of the abundant reaction $\nu_e\ ^{12}\mathrm{C} \rightarrow e^-\ ^{12}\mathrm{N}$.

LAMPF produces neutrinos from the decay of pions and muons. The predominant processes are $\pi^+ \rightarrow \mu^+ \nu_\mu$ and $\mu^+ \rightarrow e^+ \overline{\nu}_\mu \nu_e$, the decay of negative particles being suppressed by the high probability of nuclear capture. Measured pion cross sections [3] are used in the neutrino beam simulation [4], which predicts a total flux of $\overline{\nu}_\mu$ from μ decay at rest of $3 \times 10^{13} \overline{\nu}_\mu/\mathrm{cm}^2$ at the center of LSND for the 3.5 months of data analyzed, with an estimated absolute uncertainty of 7% and $\Phi_{\overline{\nu}_e}/\Phi_{\overline{\nu}_\mu} \approx 4 \times 10^{-4}$. The neutrino beam also allows a search for $\nu_\mu \rightarrow \nu_e$ oscillations [5,6] and ν_μ quasielastic interactions [7,8] because the few percent of π^+ decaying in flight give a directed beam of higher momentum ν_μ. Data for that search are not analyzed here, but the high energy ν_μ contribute to a potential background source.

The detector is an approximately cylindrical tank 8.3 m long and 5.7 m in diameter, 29.8 m from the beam production point. Inside the tank, 1220 8″ Hamamatsu phototubes (PMT) provide 25% uniform areal coverage of 157 m^3 of mineral oil doped with a small amount, 0.031 g/l, of butyl-PBD scintillator. The tank is surrounded, except on the bottom, by a high light output liquid scintillator veto shield [9] viewed by 292 5″ PMT, which detects high energy cosmic ray muons with a measured inefficiency of $\sim 2 \times 10^{-5}$. The entire apparatus is under $\sim$2000 g/cm^2 of passive shielding. A sample of $\mathcal{O}(10^6)$ electrons from cosmic ray muon decay is used to determine the energy response and resolution of the detector, as well as the efficiency of $e^{\pm}$ identification. The fractional energy resolution for electrons at 53 MeV is 8%, and at 35 MeV is 10%. A lower cut on energy of 37 MeV is applied to $e^{\pm}$ signal candidates.

Triggering decisions are based on global sums over 200 ns of detector and of veto shield PMT signal multiplicities. Events with more than 5 veto PMT signals are vetoed and initiate a veto of future events for 15.2 μs. If not vetoed, any event passing a threshold corresponding to 5 MeV electron energy in the detector is designated a primary trigger, and recorded with up to four events in the previous 52 μs that passed a threshold of 17 detector or 5 veto PMT signals. Unvetoed primaries with $\geq$125 detector PMT signals initiate a lowering of the primary threshold to 21 detector PMT for the next millisecond so that subsequent low energy gamma radiation can be detected. Event losses due to the veto shield and to the loss of events overwritten in memory total (19 $\pm$ 3)% for primaries, and 22% for γ rays.

The beam status is not used in trigger decisions, but recorded with each event, allowing detailed study of beam-unrelated backgrounds. The number expected is measured precisely because of the 7.6% ratio of beam-on time to beam-off time, and the spatial distribution of this background aids in distinguishing it from the potential signal. Particle identification is accomplished by detection of forward directed prompt light in the Čerenkov cone of relativistic particles, distinguishing them from heavier charged particles that produce isotropic, more slowly emitted scintillation light. Light and heavy particles are distinguished well by the $\chi^2/N_{\mathrm{d.f.}}$ for the reconstructed track direction fit, the $\chi^2/N_{\mathrm{d.f.}}$ for the fit to the vertex

 0031-9007/95/75(14)/2654(4)$06.00

position, and the fraction of PMT signals occurring (corrected for photon time of flight) more than 12 ns later than the reconstructed event time. This product is corrected for an observed energy dependence based on studies of the muon decay electron sample. Selection based on this single parameter is 89% efficient in accepting $e^{\pm}$ and 99% efficient in rejecting heavy backgrounds.

LSND took data for a 6 week run in 1993, with a $\overline{\nu}_{\mu}$ flux of $9 \times 10^{12} \nu/\mathrm{cm}^2$, after which the configuration of the active veto system was slightly changed; the last of the passive shielding was added, and the electronics were modified to linearize the energy response of the detector. This change in the energy response changes the energy dependence of the particle identification scheme, contributing to the incompatibility of the data from the early run and the 3.5× larger data set from 1994. Only 1994 data are used in this analysis.

The properties of neutron capture γ rays can be studied using the large flux of cosmic ray neutrons and the 186 μs capture time of neutrons in mineral oil. Requirements are placed on the energy of γ rays, their time of occurrence and distance relative to the $e^{\pm}$. It is required that the reconstructed relative distance be less than 2.4 m (the reconstruction error on γ rays is approximately 1 m), the relative time less than 750 μs ($\approx$4 capture times), and that the γ ray exhibit at least 26 detector PMT hits. The efficiency for the detection of a capture γ ray from a neutron coming from a signal event is 60%. (See Table I for the individual efficiencies.) The measured probability of an accidental $e^{\pm}$-γ coincidence passing the selection criteria is 12%. A less intuitive way to identify $e^{\pm}$-γ correlation is the use of a single likelihood ratio calculated from the above three physical quantities. An approximate likelihood variable is used in an alternative analysis.

Scatter plots of the projections of the reconstructed positions of background (i.e., beam-off) events are shown in Fig. 1. There are 1381 $e^{\pm}$ shown in the top plots, and 1961 associated γ rays shown directly below them. No $e^{\pm}$-γ coincidence is required in the data of Fig. 1 (except the 1 ms trigger requirement for any gamma that does occur; none is required), and the spatial requirement is only that the reconstructed $e^{\pm}$ be at least 30 cm from the surface defined by the PMT faces. The coordinate system is defined by taking $\hat{z}$ along the detector cylindrical axis and $\hat{y}$ vertical; the beam is along $-0.1\hat{y} + 0.99\hat{z}$. Both *Y-X* and *Y-Z* projections are shown. The surface at the PMT faces is represented by the plot frame in the *Y-Z* projections, and by the thin curve and part of the frame in the *Y-X* plots.

TABLE I. Efficiency of selection for the final sample. The efficiency of in-time veto shield and previous detector activity are measured by generating external control events with a laser. The cut on previous activity of $e^{\pm}$ is motivated by the large background of μ decay.

Cuts applied on	Acceptance
Previous activity	0.65
In-time veto for e^{+}	0.87
e^{+} particle ID	0.89
Live time for $e^{\pm}$	0.81
$e^{\pm}$-γ correlation	0.93
γ energy	0.9
In-time veto for γ	0.93
Live time for γ	0.78
Total	0.25

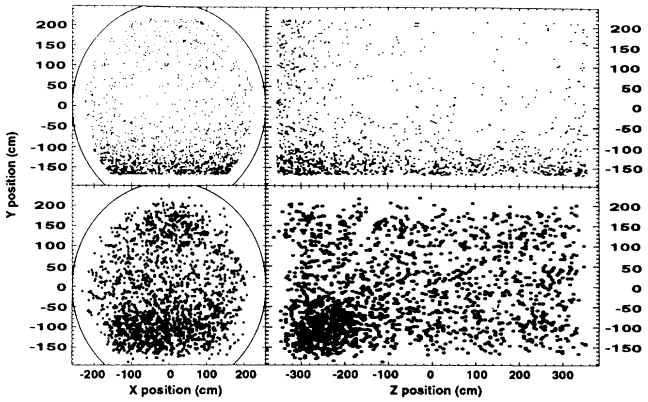

FIG. 1. Positions of the beam-unrelated backgrounds. The scatter plots show positions of individual $e^{\pm}$ (upper plots) and associated γ rays (lower plots) in *YX* and *YZ* projection. No e-γ coincidence is required for these samples, beside the 1ms time coincidence required by the on-line trigger. The tangent surface to the PMT faces is the plot boundary in the *Y-Z* projection, and the solid arcs together with the plot boundary in the *Y-X* projection. $e^{\pm}$ are restricted to the region $d_e^{\mathrm{PMT}} > 30$ cm. The distance between centers of adjacent PMT is 35 cm.

Figure 2 shows the same distributions for all (142) $e^{\pm}$ in time with the beam that pass all the final $e^{\pm}$

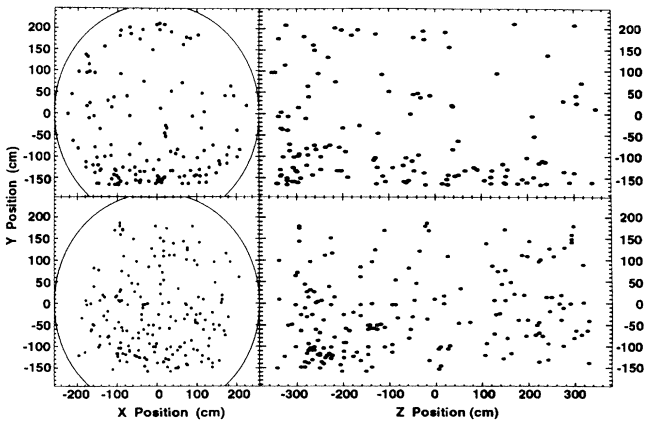

FIG. 2. Positions of the beam-on events. The 142 $e^{\pm}$ shown (upper plots) are the superset from which all e-γ coincidences must be drawn. The lower plots show the positions of the 189 γ rays that occur in the 1ms windows these electrons have initiated. The neutrino beam is along $-0.1\hat{y} + 0.99\hat{z}$. These data represent the full 4 months (5904 C) of beam.

selection criteria except a later, tighter fiducial volume requirement, and all (189) γ rays associated with these $e^{\pm}$. These events are the exact beam-on complement of the 1381 $e^{\pm}$ and 1961 γ rays shown in Fig. 1. Any $\overline{\nu}_{\mu} \rightarrow \overline{\nu}_{e}$ oscillation signal must emerge from the events in Fig. 2, after the background indicated in Fig. 1 is properly subtracted, and an $e^{\pm}$-γ coincidence required.

The inhomogeneity of the background in Fig. 1 and of the potential signal in Fig. 2 requires confining the fiducial volume to a region of the detector that is not only more background free, but within which there are no strong gradients of event density. Since the backgrounds for both $e^{\pm}$ and coincident γ are inhomogeneous, and both enhanced at the bottom of the detector, the distribution of distance between primaries and accidentally coincident γ rays will not be constant throughout the detector. This problem is addressed both by tightening the region analyzed and by the requirement that coincidences pass each of the separate criteria on $e^{\pm}$-γ relative time and distance, and γ-ray energy. A region is chosen, in part from the data in Figs. 1 and 2, and in part from separate measurements of the spatial dependence of $e^{\pm}$ detection efficiency [6], which limits the search to approximately 59 m^3 of active volume. The volume shown in Figs. 1 and 2 is reduced by 3/4 by moving inward from 30 to 50 cm from the PMT faces, and by a similar factor by excluding 1 m at the bottom of the remaining region.

Figure 3 shows the $e^{\pm}$ positions for all (25) of the beam-on events in Fig. 2 that satisfy the criteria defining a nominally coincident 2.2 MeV γ ray. Within the fiducial volume (dotted line) five events remain as possible signal candidates. Four events are concentrated just outside the periphery of the fiducial volume, and 16 near the bottom of the detector in 1/3 of the total volume analyzed. The corresponding distributions for beam-off data (not shown) have 241 $e^{\pm}$-γ coincidences, of which 43 are within the fiducial volume.

These 43 events pass all the same requirements while the beam is off, implying a background from beam-unrelated sources of $43 \times 0.076 = 3.3 \pm 0.49(\text{stat}) \pm 0.04(\text{syst})$ events. Almost as large in number is the class

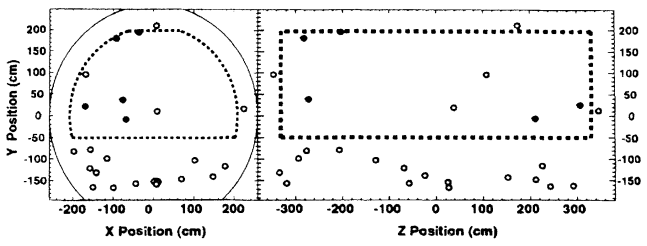

FIG. 3. The 25 beam-on e-γ coincidences, before the application of the fiducial volume cut. The fiducial region, indicated by the dotted line, is 50 cm from the PMT faces, except at the bottom of the detector, where it is 149 cm from the PMT faces. Events within this volume are denoted as solid circles, while those outside are represented as open circles. This volume is 55% of the volume represented in Figs. 1 and 2.

of events with neutrino-induced e^{-} in the correct energy range in accidental coincidence with low energy gamma radiation in the detector. These include $\nu_{\mu} e \rightarrow \nu_{\mu} e$ and $\nu_{e} e \rightarrow \nu_{e} e$, $\nu_{e}\,{}^{13}\mathrm{C} \rightarrow e^{-}\,{}^{13}\mathrm{N}$, with an end point of about 50 MeV, and $\nu_{\mu}\,{}^{12}\mathrm{C} \rightarrow \mu^{-} X$ (from higher energy neutrinos from pion decay in flight) where the muon is undetected. There are also expected to be e^{-} from $\nu_{e}\,{}^{12}\mathrm{C} \rightarrow e^{-}\,{}^{12}\mathrm{N}$, which have energy measured within 1σ of the reaction end point of 35 MeV. The excess of $e^{\pm}$ (beam-on–beam-off) satisfying all the $e^{\pm}$ selection criteria, but without a coincident γ ray is made up of these events (without an accidental γ ray) plus any beam related $e^{\pm}$ missing a real γ-ray coincidence. Both the accidental coincidence probability and the beam excess of neutrino-induced $e^{\pm}$ are measured. The background from beam-induced $e^{\pm}$ in accidental coincidence with a γ ray is calculated from these measurements as 2.5 ± 0.9. There is an expected background of events from $\overline{\nu}_{e}$ contamination from μ^{-} decay in the beam stop of about 0.3 event. Other backgrounds have been calculated, and are all found to be relatively low.

These results are stable against variation of the above selection requirements. For example, extending the region analyzed to $y = -100$ cm, i.e., 50 cm lower ($\approx$1.2 times the fiducial volume above) leaves 7 beam-on events with a background of 8.7 events. Similarly, tightening the requirement on the e-γ relative distance to 1 m (from 2.4 m) leaves only 2 beam-on events with a background of 1.5, or, setting the limit on relative time to 375 (from 750 μs) leaves 1 event with a background of 3.5.

Major backgrounds are summarized in Table II. The total background of 6.2 events leaves no apparent signal for $\overline{\nu}_{\mu} \rightarrow \overline{\nu}_{e}$ oscillations. The resulting limits on the oscillation parameters Δm^2 and $\sin^2 2\theta$ based on this number of events are shown in Fig. 4. The 90% confidence limit (C.L.) is $\sin^2 2\theta < 6 \times 10^{-3}$ for $\Delta m^2 \gtrsim 20\ \mathrm{eV}^2$ and $\Delta m^2 < 7 \times 10^{-2}\ \mathrm{eV}^2$ at $\sin^2 2\theta = 1$. Ignoring all beam-related backgrounds gives the high Δm^2 90% C.L.: $\sin^2 2\theta < 8 \times 10^{-3}$.

There is a possible signal at the limit of the detector sensitivity if one accepts events throughout almost the full detector volume, and from the run in 1993 [1]. By refining the $e^{\pm}$ particle identification by the use of cuts on the separate factors of the main parameter used here (as well as the parameter itself) one can reduce the apparent beam-

TABLE II. Expectation values for some important backgrounds. The two largest are measured (not calculated).

Background	ν source	N_{expected}
Beam-unrelated background		3.3 ± 0.5
Beam induced $e^{\pm}$ with accidental γ		2.5 ± 0.9
$\overline{\nu}_{e} p \rightarrow e^{+} n$	$\mu^{-} \rightarrow \nu_{\mu} \overline{\nu}_{e} e^{-}$	0.3 ± 0.1
$\overline{\nu}_{e} p \rightarrow e^{+} n$	$\pi^{-} \rightarrow e^{-} \overline{\nu}_{e}$	<0.01
$\nu X \rightarrow \mu n X'$	$\pi \rightarrow \mu \nu_{\mu}$ in flight	0.1 ± 0.1
	Total	6.2 ± 1.6

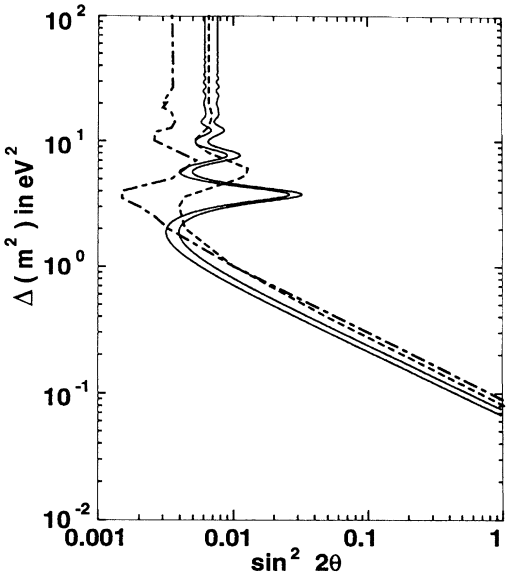

FIG. 4. Exclusion plot for mixing parameters Δm^2 and $\sin^2 2\theta$. The region to the right of and above the solid curves is excluded by this analysis at the 90(95)% confidence level. At high $\Delta(m^2)$, $\sin^2 2\Theta < 6 \times 10^{-3}$ and at full mixing $\Delta(m^2) < 0.07$ eV^2 (90% C.L.). The dash-dotted curve is the result of BNL-E776, and the dashed curve is the result from KARMEN.

unrelated background. For the purpose of identifying $e^{\pm}$-γ coincidences, a likelihood fit to the entire $e^{\pm}$ sample is done, yielding an excess of $16.4^{+9.7}_{-8.9} \pm 3.3$ events, corresponding to an oscillation probability of $0.34^{+0.20}_{-0.18} \pm 0.07$ if they are the result of $\overline{\nu}_\mu \rightarrow \overline{\nu}_e$ oscillations. While this best fit value is within the excluded region of the analysis presented here, there is a significant mutually allowed region of parameter space. Of great concern, if interpreting this as a signal, is that of the 9 events passing strict cuts on the likelihood variable (this set has an apparent total background of 2.1 ± 0.3), only 2 are in the fiducial region used in this analysis, the others falling in the regions of enhanced background.

I acknowledge the support and many fruitful discussions with A. K. Mann. I would also like to thank the members of the LSND Collaboration and the students who worked on the project, with whom most of this work was done, and the staff of LAMPF. This work is supported in part by the U.S. Department of Energy.

[1] C. Athanasopoulos *et al.*, preceding Letter, Phys. Rev. Lett. **75**, 2650 (1995).
[2] B. Pontecorve, Zh. Eksp. Theor. Phys. **33**, 549 (1957) [Sov. Phys. JETP **6**, 429 (1958)].
[3] R. C. Allen *et al.*, Nucl. Instrum. Methods Phys. Res., Sect. A **291**, 347 (1990).
[4] R. L. Burman *et al.*, Nucl. Instrum. Methods Phys. Res., Sect. A **291**, 621 (1990).
[5] W. Strossman, Ph.D. thesis, University of California, Riverside, 1995 (unpublished).
[6] J. Hill, Ph.D. thesis, University of Pennsylvania, 1995 (unpublished).
[7] Michael Albert, Ph.D. thesis, University of Pennsylvania, 1994 (unpublished).
[8] M. Albert *et al.*, Phys. Rev. C **51**, R1065 (1995).
[9] J. Napolitano *et al.*, Nucl. Instrum. Methods Phys. Res., Sect. A **274**, 152 (1989).